

Nanoscale Metal–Organic Layer Isolates Phthalocyanines for Efficient Mitochondria-Targeted Photodynamic Therapy

Geoffrey T. Nash,[#] Taokun Luo,[#] Guangxu Lan, Kaiyuan Ni, Michael Kaufmann, and Wenbin Lin*

 Cite This: *J. Am. Chem. Soc.* 2021, 143, 2194–2199

 Read Online

ACCESS |

 Metrics & More

 Article Recommendations

 Supporting Information

ABSTRACT: Zinc-phthalocyanine (ZnPc) photosensitizers (PSs) have shown great potential in photodynamic therapy (PDT) owing to their strong absorption at long wavelengths (650–750 nm), high triplet quantum yields, and biocompatibility. However, the clinical utility of ZnPc PSs is limited by their poor solubility and tendency to aggregate in aqueous environments. Here we report the design of a new nanoscale metal–organic layer (nMOL) assembly, ZnOPPC@nMOL, with ZnOPPC [ZnOPPC = zinc(II)-2,3,9,10,16,17,23,24-octa(4-carboxyphenyl)phthalocyanine] PSs supported on the secondary building units (SBUs) of a Hf₁₂ nMOL for PDT. Upon irradiation, SBU-bound ZnOPPC PSs absorb 700 nm light and efficiently sensitize the formation of singlet oxygen by preventing aggregation-induced self-quenching of ZnOPPC excited states. With intrinsic mitochondria-targeting capability, ZnOPPC@nMOL showed exceptional PDT efficacy with >99% tumor growth inhibition and 40–60% cure rates on two mouse models of colon cancer.

Photodynamic therapy (PDT) utilizes a photosensitizer (PS), light, and intratumoral oxygen to produce cytotoxic reactive oxygen species (ROS) for antitumor responses.^{1–6} Although PDT can effectively destroy local tumors with minimal systemic toxicity, its clinical utility is limited by the photophysical and pharmacokinetic properties of the PS, photosensitivity of the patient, and short tissue penetration depth of visible light.^{7–10} As highly conjugated analogues of porphyrins, phthalocyanines (PCs) possess several ideal properties as PSs: (1) strong absorption in the therapeutic window of PDT (650–800 nm) for reduced PS doses; (2) high triplet quantum yields and long triplet lifetimes in metalated PCs (M-PCs) for enhanced ROS generation; (3) high stability; (4) biocompatibility and minimal dark toxicity.^{11–13} However, few M-PCs have reached clinical testing for PDT due to their poor solubility and tendency to aggregate in aqueous environments, which induces self-quenching of excited M-PCs and significantly reduces PDT efficacy.^{14–16}

Nanoscale metal–organic frameworks (nMOFs) have shown great potential in biomedical applications.^{17–22} With structural and compositional tunability, crystallinity, framework rigidity, high porosity, and biodegradability, nMOFs have been used to incorporate PSs for PDT.^{23–26} The crystalline and rigid frameworks of nMOFs prevent photobleaching and self-quenching of PSs to significantly increase PDT efficacy.^{27,28} The dimensionality of nMOFs can be reduced to afford nanoscale metal–organic layers (nMOLs) with monolayer thickness, which further enhances ROS diffusion for cytotoxic effects on tumor cells.^{29,30} The therapeutic efficacy of PDT can also be enhanced by targeting PSs to subcellular organelles, such as mitochondria. Generation of cytotoxic ROS in mitochondria disrupts key biological processes such as energy production and activates apoptotic pathways via caspase activation.^{31–33} nMOFs with sufficient lipophilicity and

positive charge can target mitochondria^{34–36} without relying on auxiliary triphenylphosphonium moieties.^{37,38}

Herein we report the design of a Hf₁₂-Ir nMOL comprising Hf₁₂ secondary building units (SBUs) and Ir(DBB)[dF(CF₃)-ppy]₂⁺ ligands [H₂DBB-Ir-F, DBB = 4,4'-di(4-benzoato)-2,2'-bipyridine; dF(CF₃)ppy = 2-(2,4-difluorophenyl)-5-(trifluoromethyl)pyridine] for effective delivery of zinc(II)-2,3,9,10,16,17,23,24-octa(4-carboxyphenyl)phthalocyanine (ZnOPPC) PSs for mitochondria-targeted PDT (Figure 1). ZnOPPC was postsynthetically incorporated onto the nMOL via carboxylate exchange. Upon light irradiation, SBU-bound ZnOPPC PSs absorb light and undergo intersystem crossing to the triplet excited state, which, in the presence of ³O₂, efficiently generates cytotoxic ¹O₂.^{39,40} The rigid, ultrathin, and positively charged nMOL isolates ZnOPPC PSs to prevent self-quenching, while allowing efficient ROS diffusion and translocation of the nMOL into mitochondria to afford a highly effective PDT treatment of colorectal cancer.^{35,41–45}

The ZnOPPC ester was synthesized by refluxing 4,5-bis(4-methoxycarbonylphenyl)phthalonitrile, Zn(OAc)₂ and 1,8-diazabicyclo[5.4.0]undec-7-ene in *n*-pentanol for 36 h (Figure S4). High-resolution mass spectrometry (HRMS) revealed a mixture of methyl and pentyl esters in the product due to transesterification with *n*-pentanol (Figure S5). Hydrolysis of the ZnOPPC esters yielded the desired acid form of ZnOPPC. HRMS showed a single molecular ion peak with isotopic peaks matching that of ZnOPPC (Figure S8).

Received: November 25, 2020

Published: February 2, 2021



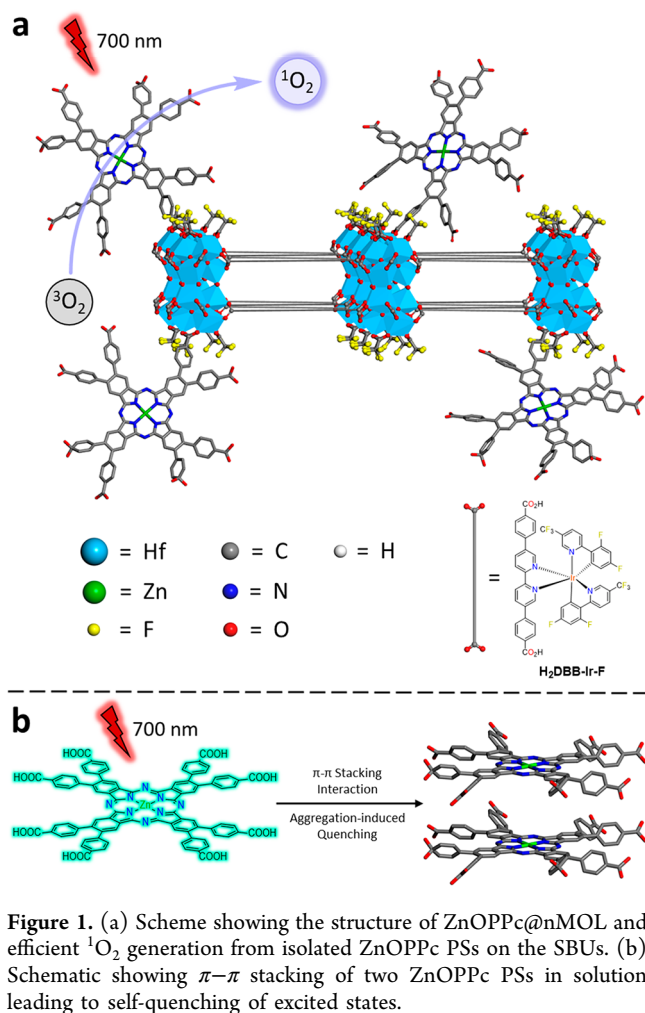


Figure 1. (a) Scheme showing the structure of ZnOPPc@nMOL and efficient $^1\text{O}_2$ generation from isolated ZnOPPc PSs on the SBUs. (b) Schematic showing π - π stacking of two ZnOPPc PSs in solution leading to self-quenching of excited states.

The UV-visible spectrum of ZnOPPc in dimethyl sulfoxide (DMSO) exhibited three peaks characteristic of ZnPc (Figure 2a).⁴⁶ The B-band peak at $\lambda_{\text{max}} = 370$ nm is assigned to a π - π^* transition with a molar extinction coefficient (ϵ) of $147\,200\text{ M}^{-1}\text{ cm}^{-1}$, which is 2–3 times lower than those of 5,10,15,20-tetra(*p*-benzoato)porphyrin (H_4TBP)⁴⁷ and 5,10,15,20-tetra(*p*-benzoato)chlorin (H_4TBC).⁴⁸ This difference may alleviate photosensitivity side-effects for ZnOPPc.^{49–51} The Q_{02} -band peak at $\lambda_{\text{max}} = 628$ nm is assigned to an n - π^* transition with $\epsilon = 61\,000\text{ M}^{-1}\text{ cm}^{-1}$, and the Q_{01} -band peak at $\lambda_{\text{max}} = 697$ nm is a π - π^* (HOMO–LUMO) transition with $\epsilon = 343\,600\text{ M}^{-1}\text{ cm}^{-1}$.⁵² The Q_{01} band has ~ 72 times larger ϵ value than the longest wavelength Q-band absorption of H_4TBP ($\epsilon_{646} = 4800\text{ M}^{-1}\text{ cm}^{-1}$). Compared to H_4TBP , the Q_{01} -band peak of ZnOPPc at 697 nm not only has a longer absorption wavelength for better tissue penetration but also has a significantly higher ϵ value because PCs lack the near-degeneracy of the a_{1u} and a_{2u} orbitals and mixing of the associated electronic configurations that led to cancellation of the transition dipole moments in porphyrins.⁵³

$\text{Hf}_{12}\text{-Ir}$ nMOL was synthesized by heating HfCl_4 and $\text{H}_2\text{DBB-Ir-F}$ in *N,N*-dimethylformamide (DMF) with trifluoroacetic acid (TFA) and water as modulators at 80°C (Figure S16).⁵⁴ ZnOPPc@nMOL was synthesized by vigorously stirring a mixture of ZnOPPc and $\text{Hf}_{12}\text{-Ir}$ nMOL in DMF/ethanol (2:1) at room temperature (Figure S16). The ZnOPPc loading was determined as 14.9 wt % based on inductively

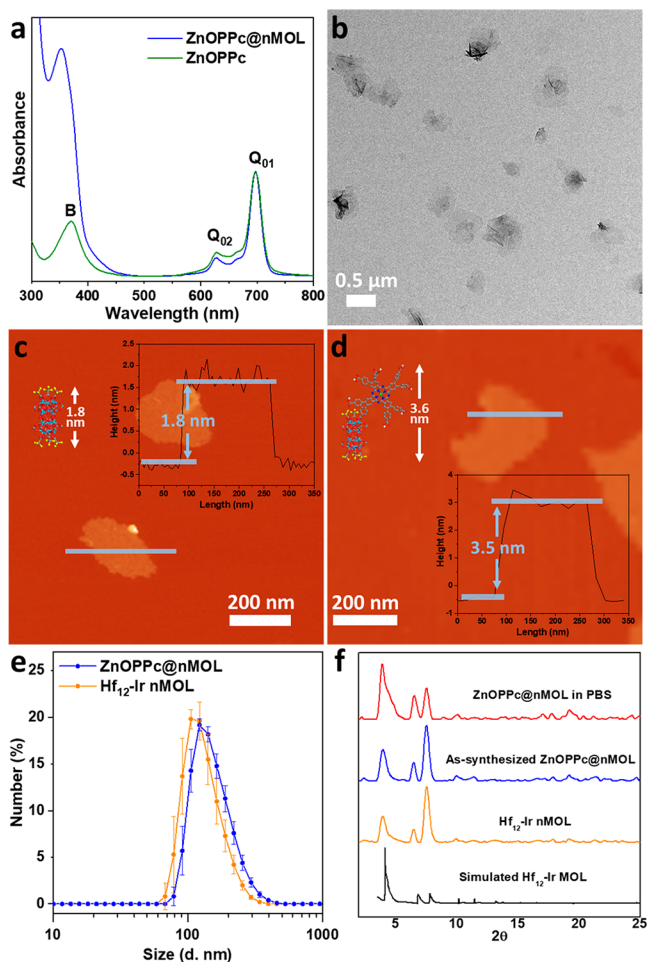


Figure 2. (a) UV-visible absorption spectra of ZnOPPc and ZnOPPc@nMOL in DMSO showing characteristic B- and Q-band peaks. (b) TEM image of ZnOPPc@nMOL. AFM topography, height profile (inset), and modeled heights of (c) $\text{Hf}_{12}\text{-Ir}$ nMOL and (d) ZnOPPc@nMOL. (e) Number-averaged diameters in ethanol and (f) PXRD patterns of $\text{Hf}_{12}\text{-Ir}$ nMOL, as-synthesized ZnOPPc@nMOL, and ZnOPPc@nMOL after soaking in PBS for 16 h, along with the simulated pattern for the Hf_{12} MOL.

coupled plasma-mass spectrometry (ICP-MS) and UV-visible absorption spectroscopy (Figure S9), which corresponds to a 1.1:1 ratio of ZnOPPc: Hf_{12} SBU. Additionally, the decrease of the TFA peak intensity in the ^{19}F NMR spectra of digested ZnOPPc@nMOL compared to the bare $\text{Hf}_{12}\text{-Ir}$ nMOL confirmed the exchange of ZnOPPc with TFA-capping ligands (Figures S18, S26). Based on these results, ZnOPPc@nMOL was formulated as $(\text{ZnOPPc})_{1.1}@\text{Hf}_{12}(\mu_3\text{-O})_8(\mu_3\text{-OH})_8(\mu_2\text{-OH})_6(\text{DBB-Ir-F})_6(\text{TFA})_{4.9}$.

Transmission electron microscopy (TEM) imaging showed that ZnOPPc@nMOL maintained the same monolayer morphology as $\text{Hf}_{12}\text{-Ir}$ nMOL (Figures 2b and S17). Atomic force microscopy (AFM) supported the monolayer structure of $\text{Hf}_{12}\text{-Ir}$ and ZnOPPc@nMOL with thicknesses of 1.8 and 3.5 nm, respectively, which are consistent with the modeled heights of Hf_{12} SBUs capped with TFA ligands (Figure 2c) and ZnOPPc (Figure 2d), respectively. Additionally, the UV-visible spectrum of ZnOPPc@nMOL showed both characteristic peaks for ZnOPPc and $\text{Hf}_{12}\text{-Ir}$ (Figure S23). Dynamic light scattering (DLS) of ZnOPPc@nMOL revealed a number-averaged size of 156.2 ± 6.4 nm with a polydispersity index of

0.10 (Figure 2e), which is slightly larger than that of Hf₁₂-Ir nMOL at 133.2 ± 8.0 nm. The cationic framework of Hf₁₂-Ir showed a highly positive zeta potential of $+36.3 \pm 0.7$ mV, while ZnOPPc@nMOL showed a negative zeta potential of -19.3 ± 1.0 mV, consistent with installation of negatively charged ZnOPPc (Figure S21). The powder X-ray diffraction (PXRD) pattern of ZnOPPc@nMOL also matched well with the experimental and simulated PXRD patterns of the bare nMOL (Figure 2f). The stability of ZnOPPc@MOL in phosphate-buffered saline (PBS) was demonstrated by PXRD and DLS after incubation at 37 °C or 700 nm LED irradiation (Figures 2f, S27, S28).

Confocal laser scanning microscopy (CLSM) imaging showed time-dependent enrichment of Hf₁₂-Ir into mitochondria of murine colorectal cancer MC38 cells. Mitochondria were labeled by MitoTracker Red CMXRos, and Hf₁₂-Ir nMOLs were detected by intrinsic fluorescence from DBB-Ir-F. At 15 min after nMOL incubation, most of the Hf₁₂-Ir fluorescence was outside of mitochondria, likely taken up and trapped in endo/lysosomes (Figure S40). From 30 min to 2 h (Figures 3a, S6b, S41, S42, S43), the fluorescence of Hf₁₂-Ir outside of mitochondria decreased, while colocalization between mitochondria and Hf₁₂-Ir signals increased, which was consistent with previous reports of mitochondria targeting by positively charged nanoparticles.^{35,41–45} Surprisingly, we observed the colocalization of ZnOPPc@nMOL with MitoTracker 30 min postincubation (Figures S3b, S41, S42, S43), likely due to reversal of surface charge for ZnOPPc@nMOL after protonation of ZnOPPc but not partial release of ZnOPPc (Figure 3d). This hypothesis was supported by a positive zeta potential of $+21.5 \pm 0.3$ mV for ZnOPPc@nMOL measured in a pH = 4 acidic buffer (Figure S22), which mimics the acidic environment of the endo/lysosome. At 2 h, the Pearson's coefficients of colocalization of ZnOPPc@nMOL and Hf₁₂-Ir nMOL with MitoTracker reached 0.838 and 0.979, respectively (Figure S44). Efficient translocation of nMOLs into mitochondria was supported by Hf ICP-MS analysis (Figure S45). Eight hours after PDT treatment of ZnOPPc@nMOL (100 mW/cm², 10 min; "+" and "-" denote with and without light irradiation, respectively), depolarization of mitochondria membrane potential and release of cytochrome *c* were observed by CLSM (Figures 4a,b, S47), indicating the disruption of mitochondria by PDT treatment with ZnOPPc@nMOL.

We then examined whether the isolation of ZnOPPc PSs on the nMOL SBUs can facilitate ROS generation and diffusion and enhance cellular uptake to elicit stronger cytotoxic effects. Singlet oxygen sensor green (SOSG) assays revealed that ZnOPPc@nMOL significantly enhanced ¹O₂ generation compared to ZnOPPc in a test tube (Figure 3e) and *in vitro* (Figures 4c, S36, S37), suggesting that conjugation of ZnOPPc PSs on the nMOL reduced aggregation-induced self-quenching. ZnOPPc was sparingly soluble and severely aggregated in serum-containing media (Figure S32). As a result, ZnOPPc@nMOL showed 12 times higher cellular uptake than ZnOPPc (Figure 3c). Owing to enhanced ¹O₂ generation, high cellular uptake, and strong mitochondria-targeting effect, ZnOPPc@nMOL(+) was highly cytotoxic with an IC₅₀ of 0.11 μM (Figures 3f, S31). In contrast, ZnOPPc(+) did not inhibit proliferation or cause morphology changes at concentrations up to 10 μM (Figures S31, S32, S33, Movies S1–S9).

PDT-induced apoptosis and immunogenic cell death were evaluated on MC38 cells by flow cytometry and CLSM.

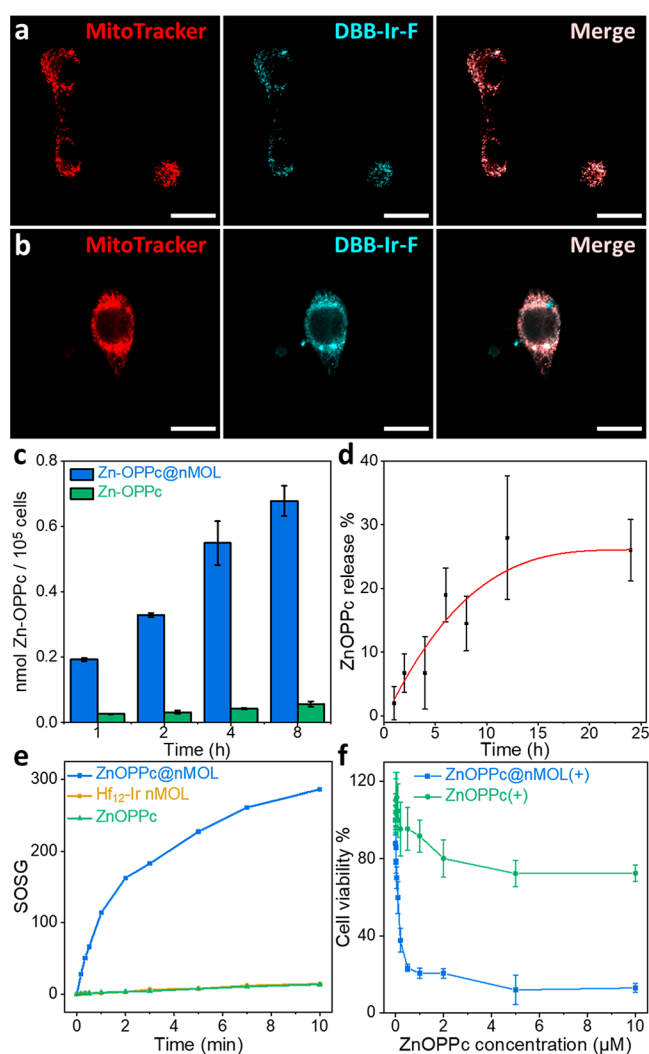


Figure 3. Hf₁₂-Ir nMOL (a) and ZnOPPc@nMOL (b) colocalized with mitochondria as visualized by CLSM after a 2 h incubation with MC38 cells (scale bars equal 20 μm). (c) Cellular uptake quantified by UV-visible spectroscopy, *N* = 3. (d) Release profile of ZnOPPc@nMOL in PBS, *N* = 3. (e) ¹O₂ generation of ZnOPPc and ZnOPPc@nMOL detected by SOSG assay. (f) MTS assay of PDT treatment with ZnOPPc or ZnOPPc@nMOL on MC38 cells, *N* = 6.

Annexin V and propidium iodine (PI) staining revealed ZnOPPc@nMOL(+) had more severe apoptotic cell death than other groups (Figures 4d, S34, S35). The ZnOPPc@nMOL(+) group also showed stronger surface translocation of calreticulin (Figures 4e, S38, S39), an "eat-me" signal during immunogenic cell death (ICD). Surface exposure of calreticulin can attract myeloid cells for phagocytosis and antigen presentation to facilitate immune responses.

The *in vivo* PDT efficacy of ZnOPPc@nMOL was evaluated on subcutaneous MC38 tumor-bearing C57BL/6 mice and CT26 tumor-bearing BALB/c mice. Hf₁₂-Ir nMOL and ZnOPPc@nMOL were PEGylated before administration. ZnOPPc, Hf₁₂-Ir, and ZnOPPc@nMOL were intravenously injected into mouse tail veins at an equivalent ZnOPPc dose of 0.1 μmol (equivalent DBB-Ir-F dose of 0.5 μmol) followed by 700 nm LED irradiation at the tumor site with a total light dose of 90 J/cm² (100 mW, 15 min). The ZnOPPc@nMOL(+) group showed superior anticancer efficacy with 99.1% and 103.8% tumor growth inhibition (TGI) on the

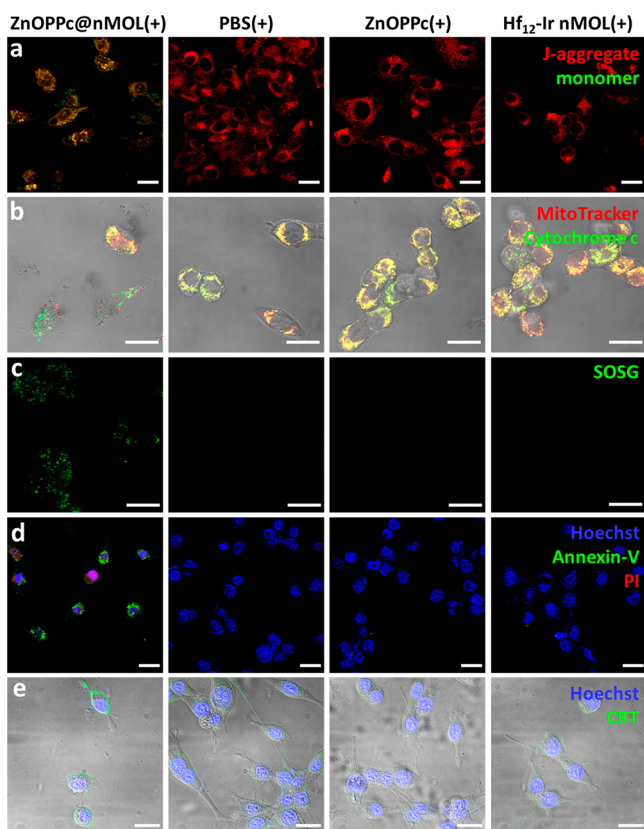


Figure 4. (a) Loss of mitochondria membrane potential by the JC-1 assay. Red channel indicates J-aggregate and green indicates monomer form of JC-1 molecules. (b) Release of cytochrome *c* (green) from mitochondria (red). (c) $^1\text{O}_2$ generation by the SOSG assay (green). (d) Cell apoptosis visualized by annexin-V (green) and PI (red) staining. (e) ICD detected by CRT expression on the cell surface (green). Cell nuclei were stained by Hoechst 33342 (blue) in (d) and (e). MC38 cells were used, and all scale bars equal 20 μm .

MC38 and CT26 model, respectively. Two out of 5 mice and 3 out of 5 mice were tumor free for MC38- and CT26-tumor-bearing mice, respectively (Figures 5a,b, S48, S49). ZnOPPc-(+) moderately inhibited tumor growth with a TGI_{MC38} of 59.6% and TGI_{CT26} of 37.7%, whereas $\text{Hf}_{12}\text{-Ir}(+)$ had a minimal effect on tumor growth with a statistically insignificant TGI_{MC38} of 35.6% and TGI_{CT26} of 10.0%. TUNEL and CRT staining revealed severe apoptosis and obvious CRT surface translocation in the ZnOPPc@nMOL(+) tumors, respectively (Figures 5c, S59, S60). ZnOPPc@nMOL(+) treatment caused severe necrosis, as shown in the H&E staining of tumor sections (Figure 5c). ZnOPPc@nMOL(+) thus exhibited pronounced antitumor activity and produced strong ICD, leading to excellent PDT efficacy. All treatment groups showed steady trends in mouse body weights (Figures S51, S56) and minimal aberration in major organ sections (Figure S55), indicating lack of general toxicity. Thus, $\text{Hf}_{12}\text{-Ir}$ nMOL is a biocompatible and efficient nanodelivery platform for PSs with significantly enhanced therapeutic effects.

In summary, we report the isolation of ZnOPPc PSs on the SBUs of cationic $\text{Hf}_{12}\text{-Ir}$ nMOLs to prevent aggregation-induced self-quenching of the excited PSs and to target mitochondria. As a result, ZnOPPc@nMOL showed significantly enhanced $^1\text{O}_2$ generation and superb anticancer efficacy over ZnOPPc. This work demonstrates the potential of using nMOLs to deliver highly potent PSs with nonideal

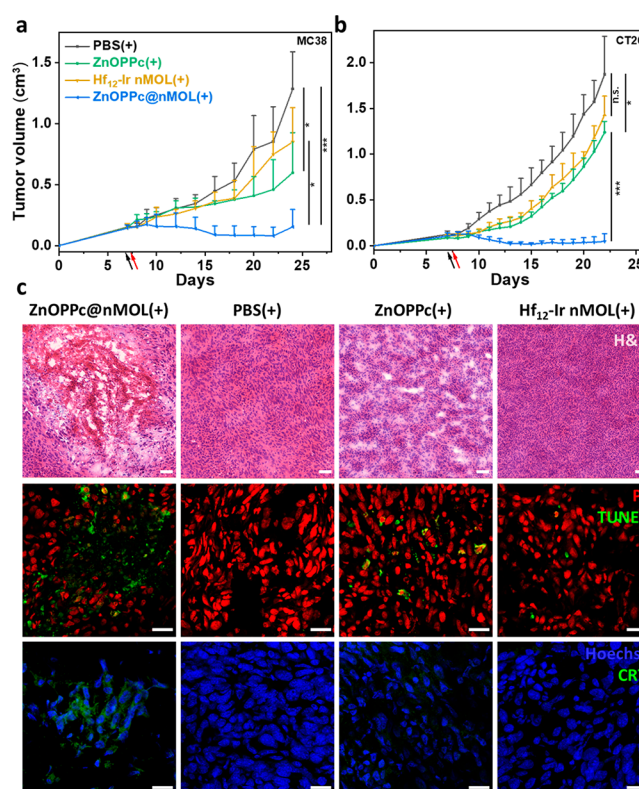


Figure 5. PDT anticancer efficacy on subcutaneous MC38 tumor-bearing C57BL/6 mice (a) and CT26 tumor-bearing BALB/c mice (b), $N = 5$. (c) H&E staining (top), TUNEL assay (middle), and CRT staining of excised tumors from treated C57BL/6 mice. Scale bars are 50 μm for H&E staining and 20 μm for the others. * $P < 0.05$ and *** $P < 0.001$ by ANOVA test.

physicochemical and pharmacokinetic properties for effective PDT treatment of cancers.

■ ASSOCIATED CONTENT

Supporting Information

The Supporting Information is available free of charge at <https://pubs.acs.org/doi/10.1021/jacs.0c12330>.

Synthesis and characterization of ZnOPPc, $\text{Hf}_{12}\text{-Ir}$ nMOL, and ZnOPPc@nMOL, ROS generation, mitochondria targeting properties, and anticancer efficacy studies (PDF)

Movie S1 (MP4)

Movie S2 (MP4)

Movie S3 (MP4)

Movie S4 (MP4)

Movie S5 (MP4)

Movie S6 (MP4)

Movie S7 (MP4)

Movie S8 (MP4)

Movie S9 (MP4)

■ AUTHOR INFORMATION

Corresponding Author

Wenbin Lin – Department of Chemistry and Department of Radiation and Cellular Oncology and Ludwig Center for Metastasis Research, The University of Chicago, Chicago, Illinois 60637, United States; orcid.org/0000-0001-7035-7759; Email: wenbinlin@uchicago.edu

Authors

Geoffrey T. Nash – Department of Chemistry, The University of Chicago, Chicago, Illinois 60637, United States;

orcid.org/0000-0002-1470-2279

Taokun Luo – Department of Chemistry, The University of Chicago, Chicago, Illinois 60637, United States;

orcid.org/0000-0001-5894-0490

Guangxu Lan – Department of Chemistry, The University of Chicago, Chicago, Illinois 60637, United States;

orcid.org/0000-0002-0415-5849

Kaiyuan Ni – Department of Chemistry, The University of Chicago, Chicago, Illinois 60637, United States;

orcid.org/0000-0002-8152-6746

Michael Kaufmann – Department of Chemistry, The University of Chicago, Chicago, Illinois 60637, United States

Complete contact information is available at:

<https://pubs.acs.org/10.1021/jacs.0c12330>

Author Contributions

#G.N. and T.L. contributed equally.

Notes

The authors declare no competing financial interest.

ACKNOWLEDGMENTS

We thank Xiaomin Jiang, Ziwan Xu, and Yingjie Fan for experimental help. We acknowledge Dr. Christine Labno for help with confocal imaging and analysis and Dr. Shihong Li for help with the histology study. We acknowledge the National Cancer Institute (U01-CA198989 and 1R01CA253655) and the University of Chicago Medicine Comprehensive Cancer Center (NIH CCSG: P30 CA014599) for funding support.

REFERENCES

- (1) Dolmans, D. E. J. G.; Fukumura, D.; Jain, R. K. Photodynamic therapy for cancer. *Nat. Rev. Cancer* **2003**, *3* (5), 380–387.
- (2) Huang, Z.; Xu, H.; Meyers, A. D.; Musani, A. I.; Wang, L.; Tagg, R.; Barqawi, A. B.; Chen, Y. K. Photodynamic therapy for treatment of solid tumors—potential and technical challenges. *Technol. Cancer Res. Treat.* **2008**, *7* (4), 309–320.
- (3) Josefsen, L. B.; Boyle, R. W. Unique diagnostic and therapeutic roles of porphyrins and phthalocyanines in photodynamic therapy, imaging and theranostics. *Theranostics* **2012**, *2* (9), 916–966.
- (4) Lovell, J. F.; Liu, T. W. B.; Chen, J.; Zheng, G. Activatable Photosensitizers for Imaging and Therapy. *Chem. Rev.* **2010**, *110* (5), 2839–2857.
- (5) O'Connor, A. E.; Gallagher, W. M.; Byrne, A. T. Porphyrin and Nonporphyrin Photosensitizers in Oncology: Preclinical and Clinical Advances in Photodynamic Therapy. *Photochem. Photobiol.* **2009**, *85* (5), 1053–1074.
- (6) Luby, B. M.; Walsh, C. D.; Zheng, G. Advanced Photosensitizer Activation Strategies for Smarter Photodynamic Therapy Beacons. *Angew. Chem., Int. Ed.* **2019**, *58* (9), 2558–2569.
- (7) Agostinis, P.; Berg, K.; Cengel, K. A.; Foster, T. H.; Girotti, A. W.; Gollnick, S. O.; Hahn, S. M.; Hamblin, M. R.; Juzeniene, A.; Kessel, D.; Korbelik, M.; Moan, J.; Mroz, P.; Nowis, D.; Piette, J.; Wilson, B. C.; Golab, J. Photodynamic therapy of cancer: An update. *Ca-Cancer J. Clin.* **2011**, *61* (4), 250–281.
- (8) Chatterjee, D. K.; Fong, L. S.; Zhang, Y. Nanoparticles in photodynamic therapy: An emerging paradigm. *Adv. Drug Delivery Rev.* **2008**, *60* (15), 1627–1637.
- (9) Lucky, S. S.; Soo, K. C.; Zhang, Y. Nanoparticles in Photodynamic Therapy. *Chem. Rev.* **2015**, *115* (4), 1990–2042.
- (10) Mallidi, S.; Anbil, S.; Bulin, A.-L.; Obaid, G.; Ichikawa, M.; Hasan, T. Beyond the Barriers of Light Penetration: Strategies,

Perspectives and Possibilities for Photodynamic Therapy. *Theranostics* **2016**, *6* (13), 2458–2487.

(11) Detty, M. R.; Gibson, S. L.; Wagner, S. J. Current Clinical and Preclinical Photosensitizers for Use in Photodynamic Therapy. *J. Med. Chem.* **2004**, *47* (16), 3897–3915.

(12) Makhseed, S.; Machacek, M.; Alfadly, W.; Tuhl, A.; Vinodh, M.; Simunek, T.; Novakova, V.; Kubat, P.; Rudolf, E.; Zimcik, P. Water-soluble non-aggregating zinc phthalocyanine and in vitro studies for photodynamic therapy. *Chem. Commun. (Cambridge, U. K.)* **2013**, *49* (95), 11149–11151.

(13) Nyokong, T. Effects of substituents on the photochemical and photophysical properties of main group metal phthalocyanines. *Coord. Chem. Rev.* **2007**, *251* (13), 1707–1722.

(14) Lo, P.-C.; Rodriguez-Morgade, M. S.; Pandey, R. K.; Ng, D. K. P.; Torres, T.; Dumoulin, F. The unique features and promises of phthalocyanines as advanced photosensitizers for photodynamic therapy of cancer. *Chem. Soc. Rev.* **2020**, *49* (4), 1041–1056.

(15) Baron, E. D.; Malbasa, C. L.; Santo-Domingo, D.; Fu, P.; Miller, J. D.; Hanneman, K. K.; Hsia, A. H.; Oleinick, N. L.; Colussi, V. C.; Cooper, K. D. Silicon phthalocyanine (pc 4) photodynamic therapy is a safe modality for cutaneous neoplasms: results of a phase I clinical trial. *Lasers Surg. Med.* **2010**, *42* (10), 888–895.

(16) Dumoulin, F.; Durmuß, M.; Ahsen, V.; Nyokong, T. Synthetic pathways to water-soluble phthalocyanines and close analogs. *Coord. Chem. Rev.* **2010**, *254* (23), 2792–2847.

(17) Lu, K.; He, C.; Guo, N.; Chan, C.; Ni, K.; Lan, G.; Tang, H.; Pelizzari, C.; Fu, Y.-X.; Spiotto, M. T.; Weichselbaum, R. R.; Lin, W. Low-dose X-ray radiotherapy-radiodynamic therapy via nanoscale metal-organic frameworks enhances checkpoint blockade immunotherapy. *Nat. Biomed. Eng.* **2018**, *2* (8), 600–610.

(18) Ni, K.; Lan, G.; Chan, C.; Quigley, B.; Lu, K.; Aung, T.; Guo, N.; La Riviere, P.; Weichselbaum, R. R.; Lin, W. Nanoscale metal-organic frameworks enhance radiotherapy to potentiate checkpoint blockade immunotherapy. *Nat. Commun.* **2018**, *9* (1), 2351.

(19) Zhang, Y.; Wang, F.; Liu, C.; Wang, Z.; Kang, L.; Huang, Y.; Dong, K.; Ren, J.; Qu, X. Nanozyme Decorated Metal-Organic Frameworks for Enhanced Photodynamic Therapy. *ACS Nano* **2018**, *12* (1), 651–661.

(20) McKinlay, A. C.; Morris, R. E.; Horcajada, P.; Férey, G.; Gref, R.; Couvreur, P.; Serre, C. BioMOFs: Metal-Organic Frameworks for Biological and Medical Applications. *Angew. Chem., Int. Ed.* **2010**, *49* (36), 6260–6266.

(21) Foucault-Collet, A.; Gogick, K. A.; White, K. A.; Villette, S.; Pallier, A.; Collet, G.; Kieda, C.; Li, T.; Geib, S. J.; Rosi, N. L.; Petoud, S. Lanthanide near infrared imaging in living cells with Yb³⁺ nano metal organic frameworks. *Proc. Natl. Acad. Sci. U. S. A.* **2013**, *110* (43), 17199.

(22) Horcajada, P.; Chalati, T.; Serre, C.; Gillet, B.; Sebrie, C.; Baati, T.; Eubank, J. F.; Heurtaux, D.; Clayette, P.; Kreuz, C.; Chang, J.-S.; Hwang, Y. K.; Marsaud, V.; Bories, P.-N.; Cynober, L.; Gil, S.; Férey, G.; Couvreur, P.; Gref, R. Porous metal-organic-framework nanoscale carriers as a potential platform for drug delivery and imaging. *Nat. Mater.* **2010**, *9* (2), 172–178.

(23) Furukawa, H.; Cordova, K. E.; O'Keeffe, M.; Yaghi, O. M. The Chemistry and Applications of Metal-Organic Frameworks. *Science* **2013**, *341* (6149), 1230444.

(24) Long, J. R.; Yaghi, O. M. The pervasive chemistry of metal-organic frameworks. *Chem. Soc. Rev.* **2009**, *38* (5), 1213–1214.

(25) Lan, G.; Ni, K.; Veroneau, S. S.; Feng, X.; Nash, G. T.; Luo, T.; Xu, Z.; Lin, W. Titanium-Based Nanoscale Metal-Organic Framework for Type I Photodynamic Therapy. *J. Am. Chem. Soc.* **2019**, *141* (10), 4204–4208.

(26) Lu, K.; Aung, T.; Guo, N.; Weichselbaum, R.; Lin, W. Nanoscale Metal-Organic Frameworks for Therapeutic, Imaging, and Sensing Applications. *Adv. Mater.* **2018**, *30* (37), 1707634.

(27) Lan, G.; Ni, K.; Lin, W. Nanoscale metal-organic frameworks for phototherapy of cancer. *Coord. Chem. Rev.* **2019**, *379*, 65–81.

- (28) Lismont, M.; Dreesen, L.; Wuttke, S. Metal-Organic Framework Nanoparticles in Photodynamic Therapy: Current Status and Perspectives. *Adv. Funct. Mater.* **2017**, *27* (14), 1606314.
- (29) Lan, G.; Ni, K.; Veroneau, S. S.; Song, Y.; Lin, W. Nanoscale Metal-Organic Layers for Radiotherapy-Radiodynamic Therapy. *J. Am. Chem. Soc.* **2018**, *140* (49), 16971–16975.
- (30) Lan, G.; Ni, K.; Veroneau, S. S.; Luo, T.; You, E.; Lin, W. Nanoscale Metal-Organic Framework Hierarchically Combines High-Z Components for Multifarious Radio-Enhancement. *J. Am. Chem. Soc.* **2019**, *141* (17), 6859–6863.
- (31) Green, D. R.; Reed, J. C. Mitochondria and Apoptosis. *Science* **1998**, *281* (5381), 1309–1312.
- (32) Neupert, W.; Herrmann, J. M. Translocation of Proteins into Mitochondria. *Annu. Rev. Biochem.* **2007**, *76* (1), 723–749.
- (33) Orrenius, S. Reactive Oxygen Species in Mitochondria-Mediated Cell Death. *Drug Metab. Rev.* **2007**, *39* (2–3), 443–455.
- (34) Cao, R.; Jia, J.; Ma, X.; Zhou, M.; Fei, H. Membrane Localized Iridium(III) Complex Induces Endoplasmic Reticulum Stress and Mitochondria-Mediated Apoptosis in Human Cancer Cells. *J. Med. Chem.* **2013**, *56* (9), 3636–3644.
- (35) Ni, K.; Lan, G.; Veroneau, S. S.; Duan, X.; Song, Y.; Lin, W. Nanoscale metal-organic frameworks for mitochondria-targeted radiotherapy-radiodynamic therapy. *Nat. Commun.* **2018**, *9* (1), 4321.
- (36) Poynton, F. E.; Bright, S. A.; Blasco, S.; Williams, D. C.; Kelly, J. M.; Gunnlaugsson, T. The development of ruthenium(ii) polypyridyl complexes and conjugates for in vitro cellular and in vivo applications. *Chem. Soc. Rev.* **2017**, *46* (24), 7706–7756.
- (37) Gao, Z.; Li, Y.; Zhang, Y.; Cheng, k.; An, P.; Chen, F.; Chen, J.; You, C.; Zhu, Q.; Sun, B. Biomimetic Platinum Nanozyme Immobilized on 2D Metal-Organic Frameworks for Mitochondrion-Targeting and Oxygen Self-Supply Photodynamic Therapy. *ACS Appl. Mater. Interfaces* **2020**, *12* (2), 1963–1972.
- (38) Liu, C.; Liu, B.; Zhao, J.; Di, Z.; Chen, D.; Gu, Z.; Li, L.; Zhao, Y. Nd³⁺-Sensitized Upconversion Metal-Organic Frameworks for Mitochondria-Targeted Amplified Photodynamic Therapy. *Angew. Chem., Int. Ed.* **2020**, *59* (7), 2634–2638.
- (39) Wei, S.; Zhou, J.; Huang, D.; Wang, X.; Zhang, B.; Shen, J. Synthesis and Type I/Type II photosensitizing properties of a novel amphiphilic zinc phthalocyanine. *Dyes Pigm.* **2006**, *71* (1), 61–67.
- (40) Çamur, M.; Durmuş, M.; Bulut, M. Highly singlet oxygen generative water-soluble coumarin substituted zinc(II) phthalocyanine photosensitizers for photodynamic therapy. *Polyhedron* **2012**, *41* (1), 92–103.
- (41) Yousif, L. F.; Stewart, K. M.; Kelley, S. O. Targeting Mitochondria with Organelle-Specific Compounds: Strategies and Applications. *ChemBioChem* **2009**, *10* (13), 2131–2131.
- (42) Lan, G.; Ni, K.; You, E.; Wang, M.; Culbert, A.; Jiang, X.; Lin, W. Multifunctional Nanoscale Metal-Organic Layers for Ratiometric pH and Oxygen Sensing. *J. Am. Chem. Soc.* **2019**, *141* (48), 18964–18969.
- (43) Murphy, M. P.; Smith, R. A. J. Drug delivery to mitochondria: the key to mitochondrial medicine. *Adv. Drug Delivery Rev.* **2000**, *41* (2), 235–250.
- (44) Weissig, V.; Boddapati, S. V.; Jabr, L.; D'Souza, G. G. Mitochondria-specific nanotechnology. *Nanomedicine* **2007**, *2* (3), 275–285.
- (45) Wongrakpanich, A.; Geary, S. M.; Joiner, M.-I. A.; Anderson, M. E.; Salem, A. K. Mitochondria-targeting particles. *Nanomedicine* **2014**, *9* (16), 2531–2543.
- (46) Ogunsipe, A.; Chen, J.-Y.; Nyokong, T. Photophysical and photochemical studies of zinc(ii) phthalocyanine derivatives—effects of substituents and solvents. *New J. Chem.* **2004**, *28* (7), 822–827.
- (47) Lan, G.; Ni, K.; Xu, Z.; Veroneau, S. S.; Song, Y.; Lin, W. Nanoscale Metal-Organic Framework Overcomes Hypoxia for Photodynamic Therapy Primed Cancer Immunotherapy. *J. Am. Chem. Soc.* **2018**, *140* (17), 5670–5673.
- (48) Lu, K.; He, C.; Guo, N.; Chan, C.; Ni, K.; Weichselbaum, R. R.; Lin, W. Chlorin-Based Nanoscale Metal-Organic Framework Systemically Rejects Colorectal Cancers via Synergistic Photodynamic Therapy and Checkpoint Blockade Immunotherapy. *J. Am. Chem. Soc.* **2016**, *138* (38), 12502–12510.
- (49) Goff, B. A.; Bachor, R.; Kollias, N.; Hasan, T. Effects of photodynamic therapy with topical application of 5-aminolevulinic acid on normal skin of hairless guinea pigs. *J. Photochem. Photobiol., B* **1992**, *15* (3), 239–251.
- (50) Wolf, P.; Rieger, E.; Kerl, H. Topical photodynamic therapy with endogenous porphyrins after application of 5-aminolevulinic acid: An alternative treatment modality for solar keratoses, superficial squamous cell carcinomas, and basal cell carcinomas? *J. Am. Acad. Dermatol.* **1993**, *28* (1), 17–21.
- (51) Menter, J. M.; Hollins, T. D.; Sayre, R. M.; Etemadi, A. A.; Willis, I.; Hughes, S. N. G. Protection against photodynamic therapy (PDT)-induced photosensitivity by fabric materials. *Photodermatol., Photoimmunol. Photomed.* **1998**, *14* (5–6), 154–159.
- (52) Mack, J.; Stillman, M. J. Band deconvolution analysis of the absorption and magnetic circular dichroism spectral data of ZnPc (–2) recorded at cryogenic temperatures. *J. Phys. Chem.* **1995**, *99* (20), 7935–7945.
- (53) Ricciardi, G.; Rosa, A.; Baerends, E. J. Ground and Excited States of Zinc Phthalocyanine Studied by Density Functional Methods. *J. Phys. Chem. A* **2001**, *105* (21), 5242–5254.
- (54) Quan, Y.; Lan, G.; Fan, Y.; Shi, W.; You, E.; Lin, W. Metal-Organic Layers for Synergistic Lewis Acid and Photoredox Catalysis. *J. Am. Chem. Soc.* **2020**, *142* (4), 1746–1751.